Measurement of the cross sections for collisional broadening of the intercombination transitions in calcium and strontium

John K. Crane, Michael J. Shaw, and R. W. Presta
Laser Program, Lawrence Livermore National Laboratory, P.O. Box 808, Livermore, California 94550
(Received 12 July 1993)

We employ an alternative technique for determining the Lorentzian linewidth based upon the simultaneous measurement of the vapor transmission and group-velocity delay outside the Doppler core of an optically dense transition. We apply this technique to measure the cross sections for broadening of the intercombination lines of calcium, $4s^2\,{}^1S_0 \rightarrow 4s4p\,{}^3P_1$, and strontium, $5s^2\,{}^1S_0 \rightarrow 5s5p\,{}^3P_1$, by collisions with argon, neon and the ground-state neutral vapor. We compare our measured results with calculated values as well as previously determined values by other workers.

PACS number(s): 32.70.Jz, 34.40.+n, 35.80.+s

I. INTRODUCTION

The measurement of spectral line shapes and collisional broadening cross sections has wide application in many areas including astrophysics, plasma and atomic physics, and gaseous electronics. The collisional broadening cross sections and the related line shapes are essential for describing radiation transport in such diverse systems as stellar atmospheres, laser-produced plasmas, the weakly ionized gas discharges found in gas lasers and fluorescent lamps, and ultranarrow-band atomic filters. In a more fundamental role, these cross sections aid in understanding the interaction potentials between colliding atoms. Several excellent reviews summarize both the experimental and theoretical status of collisional broadening and line-shape measurements as well as give specific values for many of the radiative transitions that have been measured to date [1–3].

Our need for accurate, collisional broadening cross sections was driven by an investigation into the use of resonant transitions in atomic vapors to compress frequency-chirped laser pulses [4–8]. In such a scheme the wings of an atomic resonance can easily provide tens of nanoseconds of group velocity dispersion, allowing atomic vapors to be applied to compressing pulses that are too long (>2 ns) for grating and prism techniques [9,10]. Using atomic vapors for pulse compression, a high-average-power pulse laser, such as a copper-vapor-laser (CVL) pumped dye laser that produces a 50 ns pulse, might be converted to a system with greatly enhanced peak power, expanding its potential use into areas such as x-ray lithography, high-order harmonic and incoherent, soft-x-ray generation. However, for this process to be practical, the absorption loss must be kept to a minimum, otherwise the intensity enhancement realized by the temporal compression is quickly lost due to attenuation. To minimize loss the laser pulse propagates at a frequency offset that is outside of the strongly absorbing Doppler core in the Lorentzian wing of the transition. Here, the amount of absorption for a specified amount of group velocity dispersion is directly proportional to the Lorentzian linewidth, $\Delta\nu_L$.

In this paper we describe our measurements of $\Delta\nu_L$ on the $4s^2\,{}^1S_0 \rightarrow 4s4p\,{}^3P_1$ line in Ca and the $5s^2\,{}^1S_0 \rightarrow 5s5p\,{}^3P_1$ line in Sr. We chose these transitions for several reasons: they are weak intercombination lines, so their natural and self-broadening linewidths make a small contribution to the total linewidth; their wavelengths (Sr 689.1; and Ca 657.3 nm) are suitable for efficient dye laser operation; their isotope and hyperfine structures are simple enough that either transition can be treated as a single line in the Lorentzian wing; and the vapor properties of both elements are ideal for production of high densities in a heatpipe. We describe in the following sections the experimental details of our measurement technique, the results for our measurements of the rare gas broadening and self-broadening cross sections for the Sr and Ca intercombination lines, comparing our values with other works, and finally we show semiclassical calculations for these cross sections that we compare with our measured values.

II. DESCRIPTION

Traditionally, collisional line-broadening rates are determined from line shapes by scanning a laser or monochromator across the emission or absorption line and fitting the data to a Voigt profile using a multivariable, nonlinear-least-squares fit [11]. The parameters of the fit are the Doppler and Lorentzian linewidths, the pressure-dependent frequency shift, and an amplitude scaling factor that is proportional to the product of the column density and the transition oscillator strength, Nfl. To accurately fit the line shape, this technique is limited to an approximate absorption range of 10–90%, therefore limiting the atomic density range that can be measured. In this section we describe a new technique for measuring the Lorentzian linewidth based upon a simultaneous measurement of the group velocity delay and the vapor transmission in the Lorentzian wing of the broadened line. Penkin and co-workers first developed the idea of simultaneously measuring absorption and dispersion to obtain linewidth and employed this method successfully for a variety of atomic systems [12]. In our method we

measure the Lorentzian linewidth directly without fitting the data to a line-shape function or deconvolving an instrument function; therefore data processing is very rapid, permitting us to take a few hundred data points during a single experiment. In addition the dynamic range of this technique is several orders of magnitude for Nfl [13]; consequently, we can cover a large range in density and obtain accurate values for the self-broadening linewidth as well.

In the linear propagation regime, the properties of the vapor that we want to measure, Nfl and the Lorentzian linewidth, $\Delta\nu_L$ are contained in the complex propagation vector, $k(\nu)$. We can write the real and imaginary parts of this vector as constant multiples of a complex line-shape function, $g(\nu)$, whose real and imaginary parts (g' and g'') are related by the Kramers-Kronig equations:

$$k'=k_0(n-1)=\frac{\pi}{2}r_0Nfg''(\nu)\ , \tag{1a}$$

$$k''=\frac{\sigma(\nu)N}{2}=\frac{\pi}{2}r_0Nfg'(\nu)\ . \tag{1b}$$

In Eqs. (1) $k_0=2\pi/\lambda$ is the free space propagation constant, σ is the absorption cross section, r_0 is the classical electron radius, f is the absorption oscillator strength, N is the atom density and ν is frequency. The group velocity delay (or group delay), τ_D, of a pulse traveling near in frequency to an atomic transition in a vapor, measured with respect to a pulse traveling the same distance in vacuum, is given by [13]

$$\tau_D=l\left[\frac{1}{v_g}-\frac{1}{c}\right]=\frac{l}{2\pi}\frac{\partial}{\partial\nu}[k'(\nu)]=\frac{r_0c}{4}Nfl\frac{\partial}{\partial\nu}g''(\nu,\Delta\nu)\ , \tag{2}$$

where v_g is the group velocity, c is light speed, l is the vapor path length, and $g''(\nu,\Delta\nu)$ is the imaginary part of the line-shape function. The opacity [minus the logarithm of the vapor transmission, $T(\nu)$] of the vapor near an optical transition is

$$-\ln\left[\frac{I_\nu(l)}{I_\nu(0)}\right]=-\ln[T(\nu)]=\pi r_0cNflg'(\nu)\ , \tag{3}$$

where $I_\nu(l)$ is the laser intensity transmitted through the vapor, $I_\nu(0)$ is the incident intensity at the vapor column input, and $g'(\nu)$ is the real part of the complex line-shape function. For our linewidth measurements we operated just outside of the strongly absorbing Doppler core of the Voigt profile in the Lorentzian wing. In this regime the real and imaginary parts of the line-shape function are approximately

$$g'(\nu)=\frac{1}{\pi}\frac{\Delta\nu_L/2}{(\Delta\nu_L/2)+(\nu-\nu_0)^2}\ , \tag{4a}$$

$$g''(\nu)=\frac{1}{\pi}\frac{(\nu-\nu_0)}{(\Delta\nu_L/2)+(\nu-\nu_0)^2}\ , \tag{4b}$$

where $\Delta\nu_L$ is the Lorentzian linewidth (full width at half-maximum) and $\nu-\nu_0$ is the laser frequency measured with respect to the transition line center, ν_0. Substituting Eqs. (4a) and (4b) into Eqs. (2) and (3) we can write

$$\Delta\nu_L=\frac{-\ln(I/I_0)}{2\pi\tau_D}\ , \tag{5}$$

which is valid in the Lorentzian wings of the Voigt profile when $(\nu-\nu_0)^2\gg(\Delta\nu_L/2)^2$.

The Lorentzian linewidth of a dipole transition between two atomic levels is

$$\Delta\nu_L=\frac{1}{2\pi}\left\{\frac{1}{\tau_u}+\frac{1}{\tau_l}\right\}+\frac{1}{\pi}\sum N_i\langle\sigma_i v_i\rangle\ . \tag{6}$$

The first term in brackets, called the natural linewidth, is the sum of the reciprocals of the upper and lower state radiative lifetimes. Since we are considering only ground-state transitions in this paper, we take $1/\tau_l=0$. The second term includes all collisional effects that broaden the transition linewidth. N_i is the density of the ith collision partner, σ_i is the collision cross section, and v_i is the center-of-mass velocity of the two colliders. In our measurements we include two terms in the sum in Eq. (6): $\langle\sigma_1 v_1\rangle$ for collisions between rare gas atoms and excited state metal atoms and $\langle\sigma_2 v_2\rangle$ for collisions between the excited state and ground state of the metal atom, i.e., self-broadening collisions.

The experimental setup for measuring linewidth is shown in Fig. 1. The metal vapor was generated in a 1.2 m long pipe made of 310 stainless steel that allows operation above 1000 °C. A uniform hot zone, 95 cm long, was created with a Lindberg furnace. The temperature was measured at fifteen locations along the pipe with thermocouples and recorded at regular intervals on a computer. We measured the buffer-gas pressure at room temperature with three different capacitance manometers to cover the full range in pressure of the measurements. The region of the pipe outside of the furnace was water cooled to prevent vapor condensation on the windows and to provide a rapid drop in temperature that defines the vapor column length. Although this system could be run as a heatpipe [14] we avoided operating in this mode during measurements by keeping the buffer gas pressure above the metal vapor pressure at all times. We occasionally operated the system as a heatpipe to transport metal from

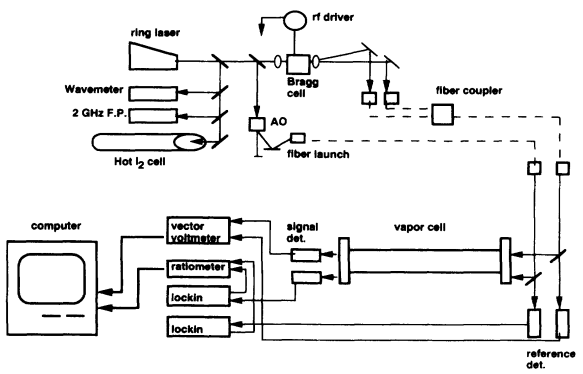

FIG. 1. Experimental setup showing ring laser, group delay diagnostic, absorption diagnostic, and frequency calibration techniques.

the cold zone back to the hot zone, but due to the rapid mass transport, this mode of operation was very unstable and unsuitable for accurate cross section measurements.

To generate the opacity and group delay probes we used a stabilized, single-frequency ring dye laser, Coherent model 699-21. The linewidth of this laser was less than 1 MHz. We used three techniques for positioning the laser near the transition of interest and generating the frequency scale. With a Burleigh wavemeter we tuned the laser within a few GHz of the transition of interest. A 60 cm long iodine cell operated at about 100 °C provided a set of reference absorption peaks whose position in frequency we carefully measured relative to line center of the calcium and strontium lines. Finally, for an accurate frequency scale we used a temperature-controlled Fabry-Pérot confocal interferometer with a 2-GHz free-spectral range.

We determined the Lorentzian linewidth outside the Doppler core by simultaneously measuring the vapor transmission and the group velocity delay over the same vapor pathlength, and calculating $\Delta\nu_L$ from Eq. (5) [13]. Both diagnostics are depicted in Fig. 1. To generate the vapor transmission (absorption) probe we split off a portion of the laser beam as shown in the layout. This transmission probe beam was amplitude modulated with an acousto-optic crystal and sent to the vapor cell via single-mode fiber. Light emerging from the fiber at the cell was again split into a reference and signal beam. The reference beam went directly to a reference photodiode detector, while the signal probe traveled through the vapor cell and illuminated the signal detector. Both detector signals were sent to lock-in amplifiers for signal conditioning before being sent to the computer. We maintained the vapor probe beam power below 10 μW to avoid optically pumping population out of the atomic lower state.

The group delay diagnostic was generated from the remainder of the laser beam that was not used for frequency calibration and the vapor transmission probe. We frequency shifted the laser using a Bragg cell and recombined the fundamental and first-order beams via single-mode fiber as shown in Fig. 1. The relative amplitudes of the two frequency components can be balanced with a polarization rotator. The beam emerging from the fiber at the vapor cell was also split into a reference and signal beam. We used the same type of photodiode detector as used for the transmission probe; however, the signal processing electronics were different. The photodiode signals were amplified with small rf amplifiers and filtered with rf bandpass filters. The resulting signal was the beat frequency between the fundamental and first order of the Bragg cell, which was driven by a high-quality, phase-locked oscillator. The signals from the reference and vapor detector were sent to a vector voltmeter—an instrument used in rf circuit analysis and testing. The vector voltmeter is capable of measuring the phase between two sinusoidal signals independent of their amplitude over several orders of magnitude. Finally, the analog output of the voltmeter was sent to the computer.

The relationship between the group velocity delay, τ_D, and the phase difference between the two detectors due to the vapor, $\Delta\phi_v$, is [13]

$$\tau_D = \frac{\Delta\phi_v}{2\pi\nu_B} , \tag{7}$$

where ν_B is the drive frequency of the Bragg cell. We operated at $\nu_B = 280$ MHz to obtain good diffraction efficiency from the Bragg cell and to match the frequency of available bandpass filters.

We acquired the data with a Macintosh computer. The computer generated a linear voltage ramp that scanned the laser over several GHz (up to 35 GHz), while simultaneously collecting signals from the group delay and vapor transmission probes, Fabry-Pérot frequency markers, iodine reference absorption peaks, plus temperature and buffer-gas pressure. The computer converted the Fabry-Pérot markers into a frequency scale, whose value with respect to the transition line center was determined from the position of the iodine peaks. Figure 2 shows a typical data set from a single laser scan. This scan was taken at a relatively low vapor density and Fig. 2(b) shows the functional form of the group delay signal as given by Eq. (2).

Most of the data were taken at large values of vapor opacity, up to several thousand, where the laser was totally absorbed at the transition line center. In this case we scanned the laser on one side of the atomic resonance as shown in Fig. 3. The discontinuities in the group delay signal, Fig. 3(a), are an instrumental effect in the vector voltmeter: when a phase difference of 180° is reached between reference and signal inputs the vector voltmeter inverts the polarity of its output voltage ("wraps-around"), which is equivalent to subtracting 2π from $\Delta\phi_v$, producing the sudden discontinuity in τ_D. The group delay signal between $\nu - \nu_0 = -10$ and 0 GHz in Fig. 3(a) is meaningless because the laser probes propagating through the vapor were completely absorbed as shown in Fig. 3(b) and therefore the signal input to the vector voltmeter was zero.

We measured the group delay and vapor transmission at two frequencies ν_1 and ν_2, in the Lorentzian wing of the atomic transition (see Fig. 3). By measuring these quantities differentially we avoid several problems associated with an absolute measurement, and we simplify the determination of the vapor density [13] and linewidth. We can easily derive the following expression for the linewidth from Eq. (5):

$$\Delta\nu_L = \frac{1}{2\pi}\frac{\ln T(\nu_1) - \ln T(\nu_2)}{\tau_D(\nu_2) - \tau_D(\nu_1)} . \tag{8}$$

So by simultaneously measuring group delay and vapor transmission at two accurately known offset frequencies, we can determine the Lorentzian linewidth quite simply and avoid the complex, multivariable analysis associated with fitting the absorption linewidth to a Voigt profile.

For each laser scan we acquired and recorded values for buffer-gas pressure, temperature, vapor transmission, and group delay at the two offset frequencies, ν_1 and ν_2. From these values we calculated the linewidth from Eq. (8) and the vapor density as described in Ref. [13]. For comparison we calculated the vapor density from the

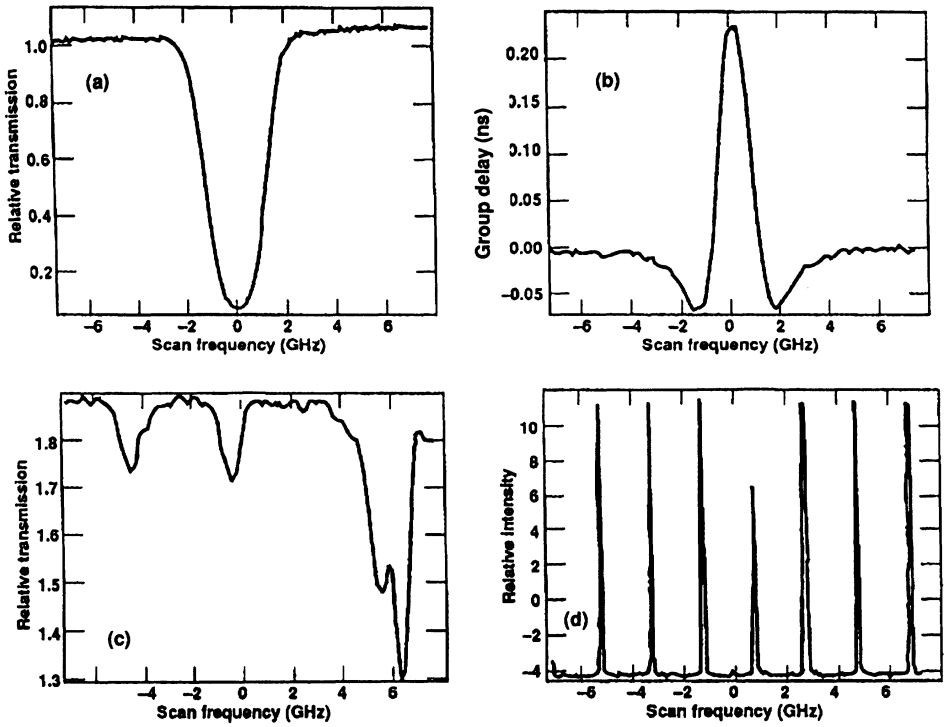

FIG. 2. Typical raw data set taken during a single laser scan: (a) calcium absorption ($4\,^1S_0 \rightarrow 4\,^3P_1$ transition at 657.3 nm); (b) calcium group delay; (c) iodine absorption; (d) 2-GHz Fabry-Pérot frequency markers.

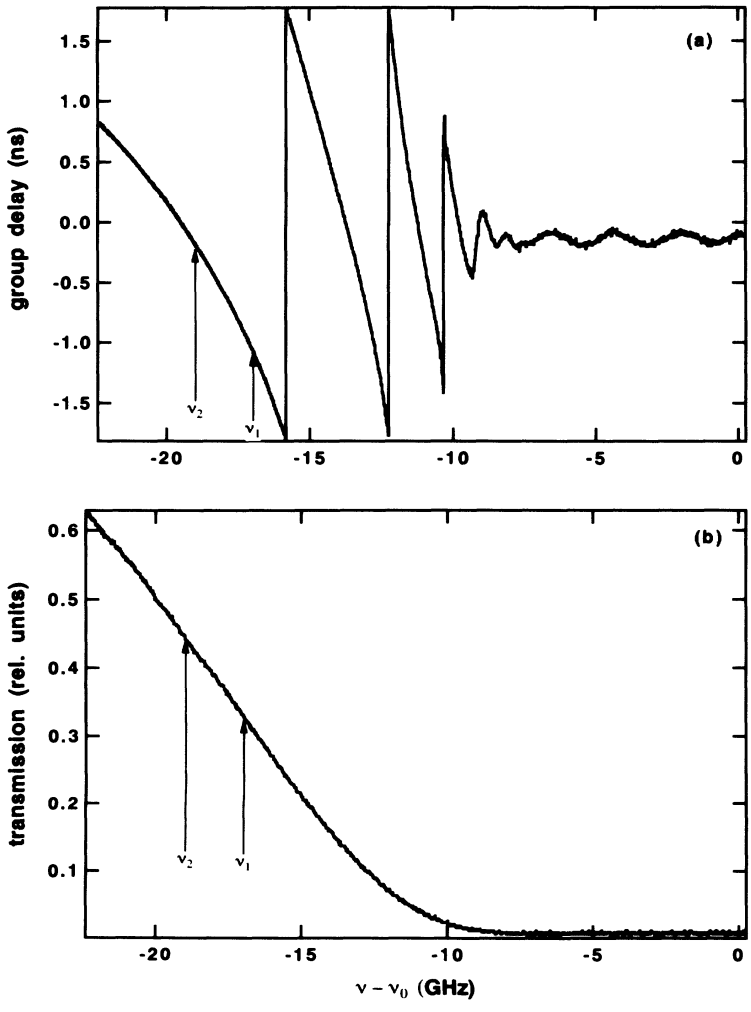

FIG. 3. Data from Sr vapor plus Ar: $N(\mathrm{Sr}) = 1.92 \times 10^{16}$ atoms/cm^3, $N(\mathrm{Ar}) = 8.72 \times 10^{16}$ atoms/cm^3, $T = 1068$ K, $\Delta\nu_L = 55.9$ MHz. (a) Group delay data show offset values, ν_1 and ν_2, used for differential measurement, and discontinuities where vector voltmeter wraps around. (b). Corresponding transmission data show opaque Doppler core and Lorentzian wing.

temperature using a polynomial fit to the vapor pressure curves [15]. All of these measured and calculated values were automatically transferred to a data base. The entire process of scanning the laser, determining the frequency scale, acquiring the measured values, calculating the vapor parameters, plotting the data, and down-loading the results into a data base took about one minute per scan.

III. RESULTS

In a typical experiment we operated the vapor cell at a constant temperature and varied the buffer-gas pressure from a value slightly above the metal vapor pressure to about 100 torr, taking several data points at pressures spanning these two limits. Figure 4 shows a plot of the linewidth of the $5s^2\,{}^1S_0 \rightarrow 5s5p\,{}^3P_1$ transition in strontium versus buffer-gas density in the hot zone, N_B (atoms/cm^3), given by

$$N_B = P\left[\frac{273}{T}\right]3.54\times10^{16} - N_v \ . \tag{9}$$

P is the pressure, in torr, read from the capacitance manometer, T is the average hot zone temperature (in Kelvins), and N_v is the vapor density determined from the group delay diagnostic. In addition to the data points we plotted a solid curve representing the linear-least-squares fit to the linewidth data. The fit is based upon Eq. (6) and yields a value for the slope,

$$k_1 = \frac{\langle \sigma_1 v_1 \rangle}{\pi} \tag{10}$$

and intercept,

$$k_0 = N_v \frac{\langle \sigma_2 v_2 \rangle}{\pi} + \frac{1}{2\pi}\frac{1}{\tau_u} \ , \tag{11}$$

where σ_1 is the cross section for broadening by collisions with the rare gas atoms, σ_2 is the cross section for collisional self-broadening via the ground-state metal atoms, and $\langle v \rangle$ is the average Maxwellian velocity between colliding atoms. The average velocity is

$$\langle v \rangle = \left[\frac{8kTN_A}{\pi}\left[\frac{1}{M_1}+\frac{1}{M_2}\right]\right]^{1/2} , \tag{12}$$

where k is Bolzmann's constant, T is the hot zone temperature, N_A is Avogadro's number, and M_1 and M_2 are the masses in atomic units of the colliding atoms.

This type of measurement, represented by Fig. 4, was repeated at several different vapor cell temperatures for each metal and buffer-gas combination. For each data set we entered the values for k_0, σ_1, $\langle v \rangle$, and T into the data base. We repeated this procedure for each of the gas-metal-vapor combinations: Ca-Ar, Ca-Ne, Sr-Ar, and Sr-Ne. Next, the values for k_0 were plotted versus the product of the metal atom density times the average velocity at each temperature as shown in Fig. 5 for strontium. As before, the solid line shown on this plot is the linear fit, yielding values for the slope and the zero density intercept. Based upon Eq. (11), the slope of this plot is σ_2/π, where σ_2 is the cross section for broadening of the dipole transition by collisions with the ground-state metal vapor, also known as self-broadening. The intercept of this linear fit is the zero density contribution to the Lorentzian linewidth—the natural linewidth. We measure a value of 668 kHz for the intercept in Fig. 5. The lifetime of the $5s^2\,{}^1S_0 \rightarrow 5s5p\,{}^3P_1$ transition in strontium is 22 μs [16], which corresponds to a linewidth of 7.23 kHz. This value is smaller than the error bar in our measurement, and consequently less than the accuracy of this technique. For stronger dipole transitions this technique may yield an accurate measurement of the radiative lifetime.

Table I gives a summary of our experimental results as well as those of other recent measurements. For the metal atom–rare gas collisions each cross section was determined from approximately 200 separate, processed laser scans covering a range of temperatures and buffer-gas pressures. For example, the Sr-Ar collisional cross section is the average calculated from 13 separate plots similar to Fig. 4, taken at 13 different temperatures between 860 and 1200 K. Each plot contains about 20 data points spanning a buffer-gas pressure range from a few torr to

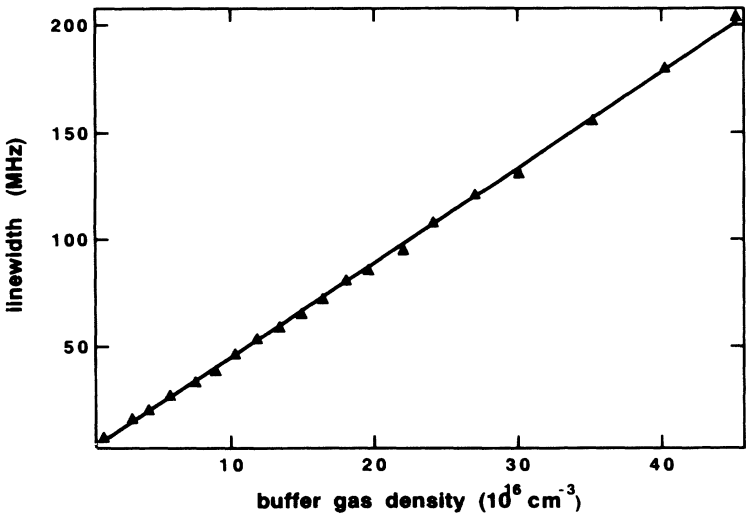

FIG. 4. Plot of measured linewidth data (triangles) versus argon density for the $5^1S_0 \rightarrow 5^3P_1$ transition in strontium at 930 K. Solid line represents the linear fit, which yields the value $\langle \sigma_1 v_1 \rangle = 1.41\times10^{-9}$ rad cm^3/s from the slope.

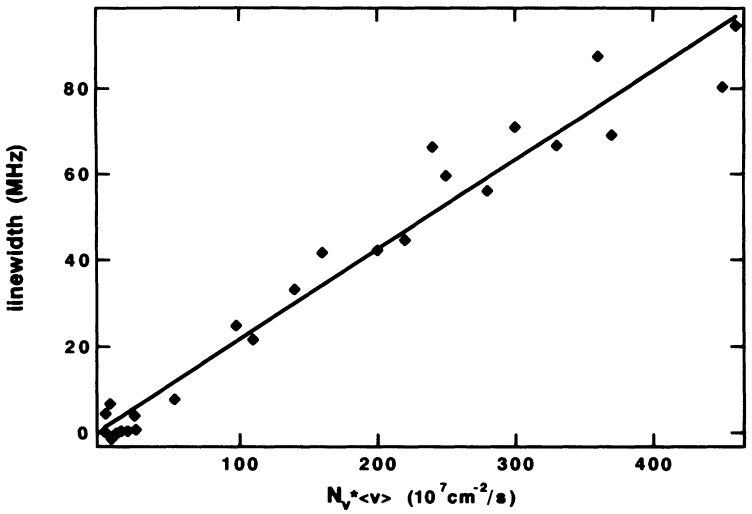

FIG. 5. Plot of the intercept values, k_0, versus the product of measured vapor density times average velocity for the $5^1S_0 \rightarrow 5^3P_1$ transition in strontium. The intercepts are taken from plots like Fig. 4 for different temperatures. The solid line is a linear fit that yields the value $\sigma_2 = 6.55 \times 10^{-14}$ cm^2.

approximately 100 torr. From each plot we determined a value for the cross section, then calculated an average and standard deviation from all of the plots representing a particular collision pair.

In searching the literature we found three previous works [17–19] that reported measured values for the widths of the Ca ($4s^2\,^1S_0 \rightarrow 4s4p\,^3P_1$) line, broadened by collisions with rare gas atoms. We compared our measured values to those reported in these references by converting their values for linewidth or collisional rate to a collisional cross section at the density and temperature of their measurement. Our values are very close to those reported by Smith [17] but differ by a factor of 2 from the more recent measurements of Rohe-Hansen [18]. In the work of Khan [19], measurements were made at two different Ar pressures and five different temperatures. We converted their linewidth at the higher Ar pressure (640 mbar) and lowest temperature (750 °C) to a collisional cross section. We selected their lowest temperature value for the comparison to minimize the self-broadening contribution, which should be less than 1% for the Ca vapor density at 750 °C. We were unable to find any reported measurements of either linewidths or collisional broadening cross sections for the Sr transition, or collisional self-broadening from either transition. Later in the paper we will compare our measured results for this transition with calculated values.

TABLE I. Summary of the measured values for the impact-broadening cross sections and comparisons with previously reported works.

Excited state	Perturber	$\sigma(10^{-14}$ cm$^2)$	Other works
Ca	Ca	0.528±0.06	
Ca	Ar	1.27±0.21	1.14[a]
			3.12[b]
			1.03[c]
Ca	Ne	0.77±0.06	0.82[a]
			1.44[b]
Sr	Sr	6.55±0.6	
Sr	Ar	1.52±0.18	
Sr	Ne	0.98±0.12	

[a]Smith [17].
[b]Rohe-Hansen and Helbig [18].
[c]Khan and Al-Kulaili [19].

The error bars given in Table I represent the purely statistical errors calculated from the linear-least-squares fits described in the previous paragraphs. In addition several experimental errors are worth discussing. In a previous work [13] we analyzed sources of noise and error in the group delay diagnostic and estimated that the combined instrumental error was about 2%. The instrumental error in the opacity measurement is comparable; therefore we estimate that the total instrumental error in measuring $\Delta\nu_L$ via Eq. (8) is 2%. This low value for the instrumental error is due primarily to the differential nature of the measurement, i.e., an absolute measurement of either opacity or group delay is more difficult and therefore would produce a larger error. The remaining sources of error arise from our determination of the cross section based upon the simple impact model represented by Eq. (6). In our measurements we have ignored the frequency shift of the transition and treated only the line-broadening effect of the collisions. For our operating range the largest collisional linewidth that we measured was 300 Mhz. For a purely van der Waals interaction between colliding atoms, the corresponding frequency shift is 107 MHz (i.e., the ratio of the linewidth to the frequency shift is -2.8 for a van der Waals interaction [20]). However, we make the differential linewidth measurement at a frequency offset of 10–20 GHz from linecenter; therefore the collisional frequency shift produces less than 1% error in the linewidth measurement.

A potentially larger source of error is the deviation of the transition wings from a purely Lorentzian shape. In Ref. [13] we discuss the error resulting from some Doppler contribution to the wings and estimate that this error is $<2\%$ for the largest value that we measured, $\Delta\nu_L/\Delta\nu_D \approx 0.5$. We also considered the effect that multiple isotopes and hyperfine structure have on the line shape. We constructed a composite Voigt line shape for the $5s^2\,^1S_0 \rightarrow 5s5p\,^3P_1$ transition using the isotope shifts and hyperfine constants found in Refs. [21,22]. The composite Voigt profile was about 20% broader in the

Doppler core, but there was no detectable difference between the single and composite lines in the region of the Lorentzian wing where we made our measurements. Since calcium is 97% Ca^{40} [23], the $4s^2\,{}^1S_0 \rightarrow 4s4p\,{}^3P_1$ transition can be accurately treated as a single line. Finally, there may be an error due to a deviation of the line shape from Lorentzian, especially at the highest densities of our measurement. We noted that at buffer-gas pressures of a several hundred torr, satellite peaks started to appear, and for this reason we limited the gas pressure to a maximum value of about 100 torr. At high buffer-gas pressures the simple impact model that we employ may not be appropriate for describing the interaction between colliding atoms and so this technique is limited to linewidth measurements where the line shape can be accurately described by a Voigt or Lorentzian function. Based upon plots such as shown in Fig. 4, we believe that a simple Lorentzian function is still accurate at the highest buffer-gas density of our measurements and that any error based upon this assumption is small.

IV. DISCUSSION

As an additional means of validating our experimental results, we compared the measured broadening cross sections to those predicted by simple classical broadening models. For the case of foreign gas broadening, the spectral broadening cross section is given by [24]

$$\sigma = 2\pi \int_0^\infty [1-\cos\eta(\rho)]\rho\, d\rho \ , \tag{13}$$

where $\eta(\rho)$ is the phase change of the classical radiating oscillator caused by a collision which occurs at an impact parameter ρ. The phase change is defined as

$$\eta(\rho) = \frac{1}{\hbar}\int_{-\infty}^{\infty} V(R)dt \ , \tag{14}$$

where $V(R)$ is the interaction potential and the interaction distance R is assumed to be

$$R^2 = \rho^2 - (\bar{v}t)^2 \tag{15}$$

corresponding to a straight line trajectory for the perturbing atom. Transforming phase change into an integral involving distance, we have

$$\eta(\rho) = \frac{1}{\hbar}\int_{-\infty}^{\infty} \frac{V(R)R\, dR}{[R^2-\rho^2]^{1/2}} \ . \tag{16}$$

For broadening by a foreign gas, we will assume that the interaction between the atoms is described by the Lennard-Jones [25] potential:

$$V(R) = \frac{C_{12}}{R^{12}} - \frac{C_6}{R^6} \ . \tag{17}$$

For this form of the interaction potential, the phase shift is given within the impact approximation by [26]

$$\eta(\rho) = \frac{63\pi}{256}\frac{C_{12}}{\hbar\bar{v}}\rho^{-11} - \frac{3\pi}{8}\frac{C_6}{\hbar\bar{v}}\rho^{-5} \ ,$$
$$\eta(\rho) = \alpha x^{-11} - x^{-5} \ , \tag{18}$$

where we have defined

$$x = \left[\frac{3\pi}{8}\frac{C_6}{\hbar\bar{v}}\right]^{-1/5}\rho \ ,$$
$$\alpha = \frac{63\pi}{256}\left[\frac{8}{3pC_6}\right]^{11/5}(\hbar\bar{v})^{6/5}C_{12} \ . \tag{19}$$

Substituting Eq. (19) into the expression for the collisional broadening cross section, Eq. (13), yields the following expression:

$$\sigma = 4\pi\left[\frac{3\pi C_6}{8\hbar\bar{v}}\right]^{2/5} B(\alpha) \ , \tag{20a}$$

$$B(\alpha) = \int_0^\infty x\sin^2\{\tfrac{1}{2}(\alpha x^{-11} - x^{-5})\}dx \ . \tag{20b}$$

The integral expression for the dimensionless number $B(\alpha)$ must be solved numerically for a given value of α. Thus, given values of C_6, C_{12} and a mean relative velocity, one can calculate α, $B(\alpha)$, and σ.

Experimentally derived values of C_6 and C_{12} have been reported by Hindmarsh [27] for both the Ca-Ne and Ca-Ar interactions. These values are listed in Table II. For a temperature of 1050 K, the relative velocities of the collision partners are 1.29×10^5 cm/sec and 1.05×10^5 cm/sec for the Ca-Ne and Ca-Ar interactions, respectively. Substituting these values into the expression for α [Eq. (19)] yields α(Ca-Ne) = 16.39 and α(Ca-Sr) = 3.92. Numerical integration of Eq. (20b) gives $B(\alpha(\text{Ca-Ne}))$ $=0.424$ and $B(\alpha(\text{Ca-Sr}))=0.316$. Substitution of these values into Eq. (20a) yields the following collisional broadening cross sections:

$$\sigma(\text{Ca-Ne}) = 0.83\times10^{-14}\ \text{cm}^2 \ ,$$
$$\sigma(\text{Ca-Ar}) = 1.19\times10^{-14}\ \text{cm}^2 \ .$$

For the foreign gas interactions involving Sr, we have been unable to find published theoretical or experimental values of C_6 and C_{12}. We can, however, approximate these using the corresponding calcium parameters and simple scaling assumptions. We recall that the dipole-dipole interaction coefficient C_6 is given by the expression [28]

$$C_6 = e^2\alpha_p\langle r_{fi}^2\rangle \ , \tag{21}$$

where α_p is the polarizability of the perturbing atom, and $\langle r_{fi}^2\rangle$ is the difference of the quantum mechanical expectation value of r^2 for the final and initial levels of the emitting atom:

$$\langle r_{fi}^2\rangle = \langle r_f^2\rangle - \langle r_i^2\rangle \ . \tag{22}$$

TABLE II. Lennard-Jones interaction coefficents used in collisional broadening calculations for calcium.

	Collison partners	
	Ca-Ne	Ca-Ar
C_6	1.13×10^{59} erg cm^{-6}	4.6×10^{-59} erg cm^{-6}
C_{12}	1.10×10^{-102} erg cm^{-12}	7.4×10^{-102} erg cm^{-12}

Further, we will approximate $\langle r^2 \rangle$ by the Unsöld formula [29]:

$$\langle r_i^2 \rangle = \tfrac{1}{2} a_0 n^{*2} \{ 5n^{*2} + 1 - 3l(l+1) \} . \quad (23)$$

In this expression, l is the angular momentum of the level, n^* is the effective principal quantum number (quantum defect), and a_0 is the Bohr radius. From this formula, we can find the ratio of C_6(Sr) and C_6(Ca) for a given perturbing atom and use the ratio to find C_6 for the strontium–rare gas interactions.

The quantum numbers of the states involved in the calcium transitions are $n_f^*(^1S_0) = 1.49$, $n_i^*(^3P_1) = 1.79$, while those for the strontium transition are $n_f^*(^1S_0) = 1.861$ and $n_i^*(^3P_1) = 1.868$. These parameters yield a ratio of

$$\frac{C_6(\mathrm{Sr}-M)}{C_6(\mathrm{Ca}-M)} = 1.49 ,$$

which, in turn, give

$$C_6(\mathrm{Sr\text{-}Ne}) = 1.68 \times 10^{-59} \text{ erg cm}^6 ,$$

$$C_6(\mathrm{Sr\text{-}Ar}) = 6.84 \times 10^{-59} \text{ erg cm}^6 .$$

To complete our analysis of foreign gas broadening for strontium, we require values for C_{12} for the two interactions. Unfortunately, we cannot use such simple scaling arguments as before since, as Hindmarsh [24] states, no simple theoretical formula exists for C_{12}. However, since C_{12} only enters in the calculation of the broadening cross section in the evaluation of $B(\alpha)$ and since $B(\alpha)$ only varies between approximately 0.2 and 0.4 for reasonable α, any errors introduced by a poor approximation of C_{12} should be small. With this in mind, we will assume that the ratio of C_6/C_{12} for the two Ca interactions are the same as for the respective Sr interactions. Within this approximation, we have

$$C_{12}(\mathrm{Sr\text{-}Ne}) = 1.63 \times 10^{-102} \text{ erg cm}^{12} ,$$

$$C_{12}(\mathrm{Sr\text{-}Ar}) = 1.01 \times 10^{-101} \text{ erg cm}^{12} .$$

At a temperature of 1050 K, the relative velocities for the interactions are 1.18×10^5 and 0.91×10^5 cm/sec for the Sr-Ne and Sr-Ar interactions, respectively. These velocities along with the interaction coefficients give

$$\alpha(\mathrm{Sr\text{-}Ne}) = 9.12 , \quad B(\alpha) = 0.379 ,$$

$$\alpha(\mathrm{Sr\text{-}Ar}) = 2.05 , \quad B(\alpha) = 0.264 ,$$

and collisional broadening cross sections of

$$\sigma(\mathrm{Sr\text{-}Ne}) = 0.91 \times 10^{-14} \text{ cm}^2 ,$$

$$\sigma(\mathrm{Sr\text{-}Ar}) = 1.23 \times 10^{-14} \text{ cm}^2 .$$

These calculated cross sections agree with our measured values to within 10% for the calcium interactions and to within 25% for the strontium interactions.

Homogeneous or self-broadening is due to the dipole-dipole interaction between the upper and lower levels of the optical transition. Lewis [2] approximated the homogeneous broadening cross section as

$$\sigma = K' \left[\frac{2J_g + 1}{2J_e + 1} \right]^{1/2} \frac{[cr_0]\lambda f}{v} \text{ cm}^2 , \quad (24)$$

where K' is a numerical constant of order 1 which accounts for the angular momentum of the states, f is the transition oscillator strength, λ is the transition wavelength, c is the speed of light, and r_0 is the classical electron radius. Using $K' = 1$ and substituting in the appropriate quantities (where a temperature 1050 K gives $v = 1.05 \times 10^5$ cm/sec and 0.742×10^5 cm/sec for Ca and Sr, respectively), in this equation yields

$$\sigma(\mathrm{Ca\text{-}Ca}) = 0.21 \times 10^{-14} \text{ cm}^2 ,$$

$$\sigma(\mathrm{Sr\text{-}Sr}) = 6.15 \times 10^{-14} \text{ cm}^2 .$$

From this analysis we see that the measured cross section for the Ca-Ca ($f = 5.1 \times 10^{-5}$ [30]) interaction is approximately 2.5 times larger than the theoretical value, while the two values for the significantly stronger Sr-Sr ($f = 1.0 \times 10^{-3}$ [16]) interaction agree reasonably well. This discrepancy is plausible since the theoretical expression is based upon a semiclassical treatment which should be valid only for larger cross sections. In the weak transition strength regime, the neglecting of higher-order terms (beyond the dipole-dipole interaction) and overlap contributions as explicitly done in this formulation is not justified. For the experimentally measured cases discussed by Lewis, (λf) varies between 60 and 2300 Å. In contrast, the transitions studied in this paper have (λf) products of 6.9 (Sr) and 0.34 (Ca). The magnitude of the Sr transition cross section as well as those studied by Lewis justify the reliance on a semiclassical formulation of the interaction. Table III summarizes our comparison of the experimentally measured cross sections with our simple theoretical values.

V. CONCLUSIONS

We have developed and demonstrated a new technique for measuring the Lorentzian linewidth of collisionally broadened, radiative transitions, based upon the simultaneous measurement of the vapor transmission and group velocity delay in the Lorentzian wing of an atomic resonance. We applied this technique to measure the broadening of the resonance, intercombination transitions in Ca, $4s^2\,{}^1S_0 \rightarrow 4s4p\,{}^3P_1$, and Sr, $5s^2\,{}^1S_0 \rightarrow 5s5p\,{}^3P_1$, by collisions with Ar, Ne, and the ground

TABLE III. Comparison of measured collisional broadening cross sections with theoretical values.

Emitting atom	Perturbing atom	σ_{meas} (10^{-14} cm^2)	σ_{theory} (10^{-14} cm^2)	Relative error
Ca	Ca	0.528	0.21	+124%
Ca	Ar	1.27	1.19	+7%
Ca	Ne	0.77	0.84	−8%
Sr	Sr	6.55	6.15	+7%
Sr	Ar	1.52	1.23	+24%
Sr	Ne	0.98	0.91	8%

state of the metal atom itself. From the linewidth we determined the collisional broadening cross sections and compared our results with those in previous publications. In addition we calculated values for these cross sections using a classical impact model where we assume that the interaction between colliding atoms can be described by a Lennard-Jones potential. The calculated values are very close to our experimental results except in the case of self-broadening of the Ca transition, where the assumption of a purely dipole transition may not be valid. We believe that this technique is very accurate in the pressure regime where the broadened transition is truly Lorentzian, and that the simplicity derived from making simultaneous measurements of the real and imaginary index is an advantage over traditional methods that fit a Voigt profile to the absorption or emission line shape.

ACKNOWLEDGMENTS

We gratefully recognize the help we received from Jeff Paisner, Mike Johnson, Herb Friedman, John Christensen, and Diane Cooke. This work was performed under the auspices of the U.S. Department of Energy at Lawrence Livermore National Laboratory under Contract No. W-7405-ENG-48.

[1] N. Allard and J. Kielkopf, Rev. Mod. Phys. **54**, 1103 (1982).
[2] E. L. Lewis, Phys. Rep. **58**, 1 (1980).
[3] S. Y. Chen and M. Takeo, Rev. Mod. Phys. **29**, 20 (1957).
[4] D. Grischkowsky, Appl. Phys. Lett. **25**, 566 (1974).
[5] J. K. Wigmore and D. Grischkowsky, IEEE J. Quantum Electron. **14**, 310 (1978).
[6] B. Y. Zel'dovich and I. I. Sobel'man, Pis'ma Zh. Eksp. Teor. Fiz. **13**, 257 (1971) [JETP Lett. **13**, 182 (1971)].
[7] J. E. Bjorkholm, E. H. Turner, and D. B. Pearson, Appl. Phys. Lett. **26**, 564 (1975).
[8] M. J. Shaw and J. K. Crane, IEEE J. Quantum Electron. **28**, 921 (1992).
[9] E. B. Treacy, Phys. Lett. **28A**, 252 (1968).
[10] J. A. Giordmaine, M. A. Duguay, and J. W. Hansen, IEEE J. Quantum Electron. **4**, 252 (1968).
[11] There are several good descriptions of this standard technique in the recent literature: E. Ehrlacher and J. Huennekens, Phys. Rev. A **46**, 2642 (1992); Y. C. Chan and J. A. Gelbwachs, J. Phys. B **25**, 3601 (1992); M. Kotteritzsch, W. Gries, and A. Hese, *ibid.* **25**, 913 (1992).
[12] N. P. Penkin and L. N. Shabanova, Opt. Spectrosc. **23**, 11 (1966); Y. I. Ostrovskii and N. P. Penkin, *ibid.* **11**, 1 (1961); N. P. Penkin and L. N. Shabanova, *ibid.* **26**, 191 (1969).
[13] J. K. Crane, R. W. Presta, J. J. Christensen, J. D. Cooke, M. J. Shaw, M. A. Johnson, and J. A. Paisner, Appl. Opt. **30**, 4289 (1991).
[14] C. R. Vidal and J. Cooper, J. Appl. Phys. **35**, 1990 (1969).
[15] G. L. Weissler and R. W. Carlson, *Methods of Experimental Physics* (Academic, New York, 1979), Vol. 14, pp. 347–351.
[16] M. D. Havey, L. C. Balling, and J. J. Wright, Phys. Rev. A **13**, 1269 (1976).
[17] G. Smith, Proc. R. Soc. London **A297**, 288 (1967).
[18] J. Rohe-Hansen and V. Helbig, J. Phys. B **25**, 71 (1992).
[19] M. A. Khan and M. F. Al-Kuhalii, J. Phys. B **26**, 393 (1993).
[20] W. R. Hindmarsh, Mon. Not. R. Astron. Soc. **119**, 11 (1959).
[21] G. Putlitz, Z. Phys. **175**, 543 (1963).
[22] D. Bender, H. Brand, and V. Pfeufer, Z. Phys. A **318**, 291 (1984).
[23] *Handbook of Chemistry and Physics,* 48th ed., edited by R. C. Weast (CRC Press, Cleveland, OH, 1968).
[24] W. R. Hindmarsh and J. M. Farr, Prog. Quantum Electron. **2**, 141 (1972).
[25] I I. Sobelman, L. A. Vainshtein, and E. A. Yukov, *Excitation of Atoms and Broadening of Spectral Lines* (Springer-Verlag, Berlin, 1981).
[26] W. Behmenburg, J. Quant. Spectrosc. Radiat. Transfer **17**, 311 (1964).
[27] W. R. Hindmarsh, A. D. Petford, and G. Smith, Proc. R. Soc. London **A197**, 296 (1967).
[28] W. R. Hindmarsh and J. M. Farr, J. Phys. B **2**, 1338 (1969).
[29] A. Unsöld, *Physik der Sternatmosphären* (Springer, Berlin, 1955).
[30] W. L. Wiese, M. W. Smith, and B. M. Miles, *Atomic Transition Probabilities,* Natl. Stand. Ref. Data Ser., Natl. Bur. Stand. (U.S.) Circ. No. 22 (U.S. GPO, Washington, D.C., 1969).